IEEE Robotics and Automation Letters (RA-L) paper, presented at ICRA 2026, Vienna, Austria. Cite as RA-L paper.

Real-Time Communication Relay Planning With a Low-Complexity Network Quality Prediction Model in Dynamic Indoor Missions

Jaemin Seo[1], Jongyun Kim[2], Seunghwan Kim[1], Changseung Kim[1], Woojae Shin[3], and Hyondong Oh[3*]

***Abstract*—Relay robots are crucial for extending communication when a client robot performs long-range missions. However, existing network quality prediction models and relay planning methods often struggle with real-time operation due to their high computational cost and poor adaptability to frequently changing missions. To address this, we propose a real-time communication relay system featuring two key contributions. First, a low-complexity network quality prediction model using Kalman filter-based Gaussian process regression achieves efficient online inference with constant-time updates ($\sim 0.02s$). Second, a hierarchical relay planning strategy, employing a Monte Carlo tree search-based sequential planner, generates communication-aware trajectories satisfying network constraints at discrete steps. Real-world experiments validate our system's effectiveness, demonstrating near-continuous network availability (99.1% channel reliability) and boosting the packet delivery ratio from a baseline of 44.7% to 73.7%. Our integrated approach offers a practical and robust solution for dynamic indoor missions.**

***Index Terms*—Multi-robot systems, networked robots, communication relay, online network prediction.**

I. Introduction

Mobile robots are increasingly essential for critical missions in complex environments, including exploration and reconnaissance. To execute its mission, the mobile robot (client) should visit a sequence of mission points issued online by a ground control station (GCS) and report completion to receive the next assignment, which requires reliable bi-directional communication. However, the physical range of onboard radios is limited; in indoor environments, walls and structural elements cause interference that significantly reduces the effective communication distance, thereby severely constraining the feasible mission area. Without external infrastructure (e.g., access points) and with a stationary GCS endpoint, we can extend the operational range of a single client robot by deploying additional relay robots that locate themselves between the GCS and the client to forward data.

As a common approach, reactive placement of static relays when the signal degrades is employed [1], but with frequently changing mission points, this approach struggles to optimize relay placement due to its stationary nature. We therefore employ a mobile chain-formation strategy where the robots self-organize a multi-hop backbone that preserves end-to-end connectivity between the GCS and the client [2].

Effective operation of this communication system requires addressing two coupled difficulties: (i) the accurate prediction of network quality and (ii) the optimization of relay placement to reliably maintain required data throughput. In indoor environments in particular, obstacles introduce irregular signal attenuation, which complicates network quality prediction and increases the complexity of the solution space for optimal relay placement [3].

To address these challenges, we propose a relay planning system with the following contributions:

1) We proposed a low-complexity network prediction model that leverages a Kalman filter-based GPR (KF-GPR) framework [4] with reduced input dimensions, enabling efficient and accurate online prediction of network quality in complex indoor environments;
2) We develop a hierarchical relay planning strategy that combines signal-based relay position optimization with communication-aware sequential planning via Monte Carlo tree search (MCTS) [5]; and
3) Through simulations and real indoor experiments, we demonstrate that the proposed real-time relay system significantly improves network prediction accuracy and maintains stable connectivity even when mission points dynamically change.

II. Related Work

A. Network Quality Prediction

Network quality is often delegated by the received signal strength indicator (RSSI), which empirically correlates with

Manuscript received: July, 6, 2025; Revised: September, 23, 2025; Accepted: October, 20, 2025.

This paper was recommended for publication by Editor M. Ani Hsieh upon evaluation of the Associate Editor and Reviewers' comments. This research was supported by the Technology Innovation Program(No. 20018110, "Development of a wireless teleoperable relief robot for detecting searching and responding in narrow space") funded By the Ministry of Trade, Industry & Energy(MOTIE, Korea), the Korea Research Institute for defense Technology planning and advancement(KRIT) grant funded by the Korea government(DAPA(Defense Acquisition Program Administration)) (No. KRIT-CT-22-064-00, "Tactical Swarm Unmanned Aerial Vehicle Mission Planning and Autonomous Mission Replanning Technology"), and the Air Force Office of Scientific Research under award number FA9550-19-1-7032. The opinions, findings, and conclusions expressed in this work are those of the authors and do not necessarily reflect the views of the United States Air Force. (Corresponding author: Hyondong Oh)

[1]Department of Mechanical Engineering, Ulsan National Institute of Science and Technology (UNIST), Ulsan 44919, Republic of Korea (e-mail: qkek1019@unist.ac.kr; kevin6960@unist.ac.kr; pon02124@unist.ac.kr).

[2]Department of Mechanical Aerospace and Civil Engineering, University of Manchester, Oxford Rd M13 9PL, The United Kingdom. (e-mail: jongyun.kim@manchester.ac.uk).

[3]Department of Mechanical Engineering, Korea Advanced Institute of Science and Technology (KAIST), Daejeon 34051, Republic of Korea. (e-mail: oj7987@kaist.ac.kr; h.oh@kaist.ac.kr).

Digital Object Identifier (DOI): see top of this page.

IEEE Robotics and Automation Letters (RA-L) paper, presented at ICRA 2026, Vienna, Austria. Cite as RA-L paper.

packet delivery rate, throughput, and latency [6]. Indoor RSSI modeling has been studied extensively [7], [8]. High-fidelity approaches include deterministic ray-tracing and empirical multi-wall models. Ray-tracing achieves high accuracy by explicitly simulating wave propagation, but requires CAD-level geometric and material parameters, and its runtime is typically prohibitive for online use [9]. Multi-wall models reduce complexity by parameterizing penetration losses, yet they still rely on site-specific calibration (e.g., wall composition and thickness) [10]. For robotics applications that must operate online with limited prior knowledge of geometry and materials, simplified models are therefore preferred to balance accuracy with real-time performance [6], [11]. These models rely on simplified parameters that represent attenuation as a function of distance between two nodes and environmental factors, and it is crucial to optimize the parameters based on RSSI measurements to reflect actual signal loss characteristics. While such models capture the general trend of signal decay, they are limited in accounting for the noise and variability inherent in RSSI measurements. To address this limitation, hybrid models have been proposed that combine the path loss model with Gaussian process regression (GPR), enabling probabilistic and more robust predictions of RSSI [12], [13]. Nonetheless, achieving accurate GPR-based prediction is challenging due to the high-dimensional input space, which includes both transmitter and receiver coordinates. Because signal attenuation depends on the relative positions of each transmitter–receiver pair, the model must be trained on a wide range of location combinations to generalize effectively. This necessitates a large number of training samples, and since GPR scales cubically with the data size, the computational burden quickly becomes expensive for real-time applications.

B. Relay Placement Strategy

Among the wireless sensor networks literature offering various approaches, we mainly review the chain-formation relay strategy, focusing on its application to the specific challenge of sustaining a bidirectional link for a single client; Several studies optimize relay placement based on the GCS and the client's current location. For instance, Gao *et al.* [14] presented an approach that constructs a rapidly expanding random tree (RRT)-based shortest path between two endpoints (i.e., the location of the GCS and the client) and uniformly initializes relay candidates along the path. The candidates are then iteratively refined using a virtual force derived from the RSSI differences between neighboring nodes. A similar decentralized strategy is proposed in which each relay robot adjusts its position using a virtual force-based local controller [15]. Although these studies work effectively when the client moves slowly or its mission point remains relatively static, they face limitations in environments where the client's mission point can change frequently or continuously. To address this, alternative approaches optimize relay placement with respect to the anticipated mission point of the client rather than its current position. In this context, Varadharajan *et al.* [16] generate the shortest path from the GCS to the mission point and segment it into intervals, then assign relay robots to each segment. Each robot (including the client) performs decentralized local planning to move toward its assigned location while preserving the chain connectivity. However, this strategy that relies solely on local control (without long-term global planning) can converge to suboptimal configurations in complex, dynamic environments. Stephen *et al.* [17] proposed a coordinated global planning by constructing an RRT in the joint state space of all robots. The tree is expanded only when the sampled nodes meet communication connectivity constraints. After feasible joint paths are obtained, each robot moves toward its assigned relay position using a gradient-based decentralized controller. This approach enhances the guarantee of end-to-end connectivity over global paths; however, the expensive computational burden of planning in a high-dimensional joint space poses challenges for real-time deployment.

III. Preliminaries

This section reviews essential definitions for network quality prediction (Section III-A) and chain network relay planning (Section III-B). Consider a set of mobile robots indexed by the set $\mathcal{N} = \{0, \dots, R\}$, where R denotes the client robot, and the index 0 represents the GCS. Relay robots are denoted as $\mathcal{N}_{\text{relay}} = \{1, \dots, R-1\}$. The state of each robot r at time t is indicated by $\mathbf{x}_r(t) = [x_r(t), y_r(t)] \in \mathcal{X}$, where $\mathcal{X}$ represents the feasible operational space. The joint states of the entire robots are represented by $\mathbf{X}(t) = \{\mathbf{x}_r(t) | r \in \mathcal{N} \backslash \{0\}\}$.

A. Network Quality Prediction With GPR

We focus on heavily obstructed indoor settings (e.g., concrete partitions) with high penetration loss, where connectivity is governed by corridor-guided propagation. Accordingly, we adopt a dominant path model [18] whose few interpretable parameters can be calibrated online. For brevity, we denote the RSSI model between nodes a and b by $P_{a,b}$ (i.e., $P_{\text{RSSI}}(a,b) \equiv P_{a,b}$). The dominant-path model that jointly considers the Euclidean distance $d^E_{a,b} = d^E(\mathbf{x}_a, \mathbf{x}_b)$ and the obstacle-aware shortest distance $d^S_{a,b} = d^S(\mathbf{x}_a, \mathbf{x}_b)$ between any two nodes $\mathbf{x}_a$ and $\mathbf{x}_b$ ($a, b \in \mathcal{N}$), thereby capturing indoor diffraction and reflection effects as:

$$\begin{aligned} P_{a,b} &= P(\mathbf{x}_{a,b}; n, \alpha), \\ &= P_0 - 10n \log_{10}\left(d^E_{a,b}\right) - \alpha \log_{10}\left(\bar{d}_{a,b} + 1\right), \end{aligned} \tag{1}$$

where P_0 is a reference RSSI at $1\,\text{m}$, n is the path loss exponent, α quantifies the signal attenuation due to obstacles, $\mathbf{x}_{a,b} = [x_a, y_a, x_b, y_b]^\mathsf{T}$, and $\bar{d}_{a,b} = |d^E_{a,b} - d^S_{a,b}|$. By associating obstacle-induced attenuation with the path excess $\bar{d}_{a,b}$, this formulation captures the attenuation caused by intervening structures. RSSI measurements, however, could be corrupted by noise; incorporating GPR is known to be a promising solution to model the measurement noise [6]. In conventional methods, the GPR training dataset consists of node pairs $\mathbf{X}_M = \{\mathbf{x}^i_{a,b}\}_{i=1}^M$ and the corresponding RSSI measurements $\mathbf{z}_M = \{z^i_{a,b}\}_{i=1}^M$, where $a, b \in \mathcal{N}$, and M is the number of measurements. Each RSSI measurement is modeled as a noisy observation of the dominant-path model:

$$z_{a,b} = f(\mathbf{x}_{a,b}) + P(\mathbf{x}_{a,b}; n, \alpha) + \epsilon, \;\; \epsilon \sim N(0, \sigma_n^2), \tag{2}$$

where $f(\mathbf{x}) \sim \mathcal{GP}(0, k(\mathbf{x}, \mathbf{x}'))$ captures spatial variations that are not explained by (1), and $k(\cdot, \cdot)$ is a kernel function that

IEEE Robotics and Automation Letters (RA-L) paper, presented at ICRA 2026, Vienna, Austria. Cite as RA-L paper.

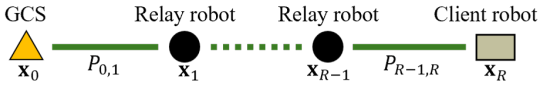

Fig. 1. A chain network topology between a client and a GCS.

defines the spatial correlation between inputs [19]. With this measurement model, the predictive distribution of RSSI at a query input $\mathbf{x}^*_{a,b} = [x^*_a, y^*_a, x^*_b, y^*_b]^\mathsf{T}$ is represented as:

$$\begin{aligned}\mu(\mathbf{x}^*_{a,b}) &= P(\mathbf{x}^*_{a,b}; n, \alpha) + \mathbf{k}_*^\mathsf{T}\mathbf{C}_M^{-1}\bar{\mathbf{z}}_M,\\ \sigma^2(\mathbf{x}^*_{a,b}) &= \mathbf{k}(\mathbf{x}^*_{a,b}, \mathbf{x}^*_{a,b}) - \mathbf{k}_*^\mathsf{T}\mathbf{C}_M^{-1}\mathbf{k}_*,\end{aligned} \tag{3}$$

where $\mathbf{C}_M = k(\mathbf{X}_M, \mathbf{X}_M) + \sigma_n^2\mathbf{I} \in \mathbb{R}^{M\times M}$, $\mathbf{k}_* = k(\mathbf{X}_M, \mathbf{x}^*_{a,b})$, and $\bar{\mathbf{z}}_M = \mathbf{z}_M - P(\mathbf{X}_M; n, \alpha)$. The most suitable parameters (n, α) are obtained by maximizing the marginal likelihood [20]:

$$\begin{aligned}\log p(\mathbf{z}_M; \mathbf{X}_M, n, \alpha) =& \bar{\mathbf{z}}_M^\mathsf{T}\mathbf{C}_M^{-1}\bar{\mathbf{z}}_M + \log|\mathbf{C}_M|\\ &+ (n+\alpha)\log 2\pi.\end{aligned} \tag{4}$$

This pipeline decouples training from parameter optimization; both require inverting $\mathbf{C}_M$ and thus scale as $\mathcal{O}(M^3)$.

B. Chain-Formation Relay System

In a chain-formation relay system (Fig. 1), relay robots forward data from the client robot to the GCS. Since a failure or degradation on any hop can cause end-to-end outages, the overall communication is governed by the bottleneck (weakest) link. Accordingly, the end-to-end network quality is determined by the minimum RSSI along the chain:

$$\bar{P}_c\left(\mathbf{X}(t)\right) = \min\left\{P_{0,1}(t), P_{1,2}(t), \ldots, P_{R-1,R}(t)\right\}. \tag{5}$$

Given a mission point, the relay system must ensure that the end-to-end network quality remains above a predefined threshold η while the client robot navigates toward the mission point $\mathbf{x}^\star_R$. To achieve this objective, it is necessary to jointly determine the trajectories of the client and the relay robots such that both the navigation goal and the communication constraints are satisfied, formulated as:

$$\begin{aligned}\mathbf{X}^\star(\mathcal{T}) = \underset{\mathbf{X}(\mathcal{T})}{\arg\min} &\int_{\mathcal{T}} ||\dot{\mathbf{x}}_R(t)||dt + \gamma\Psi(\mathbf{x}_R),\\ s.t.\ \ &\bar{P}_c(\mathbf{X}(t)) \geq \eta,\ \ \forall t \in \mathcal{T},\end{aligned} \tag{6}$$

where γ is a large weight parameter for reaching a mission point, $\mathcal{T} := [0, t_f]$ is the operation time, and $\Psi(\mathbf{x}_R) = d^S(\mathbf{x}_R(t_f), \mathbf{x}^\star_R)$. This optimization encodes the objective of navigating the client to its mission point while maintaining end-to-end connectivity via relay robots.

IV. Proposed Methodology

This section introduces our methodology, which is composed of two key components: a real-time network quality prediction model and a hierarchical relay planning strategy, jointly designed for indoor environments. The overall architecture of this integrated system is illustrated in Fig. 2. The proposed approach first establishes an efficient network quality model capable of online operation with reduced input dimensions. Subsequently, the hierarchical planner utilizes this predictive model to generate communication-aware trajectories, ensuring end-to-end connectivity as robots navigate toward their goals. Then, the robots perform onboard low-level control to follow these goals, handling collision avoidance locally. The details of the proposed system are described in the following Section IV-A and Section IV-B.

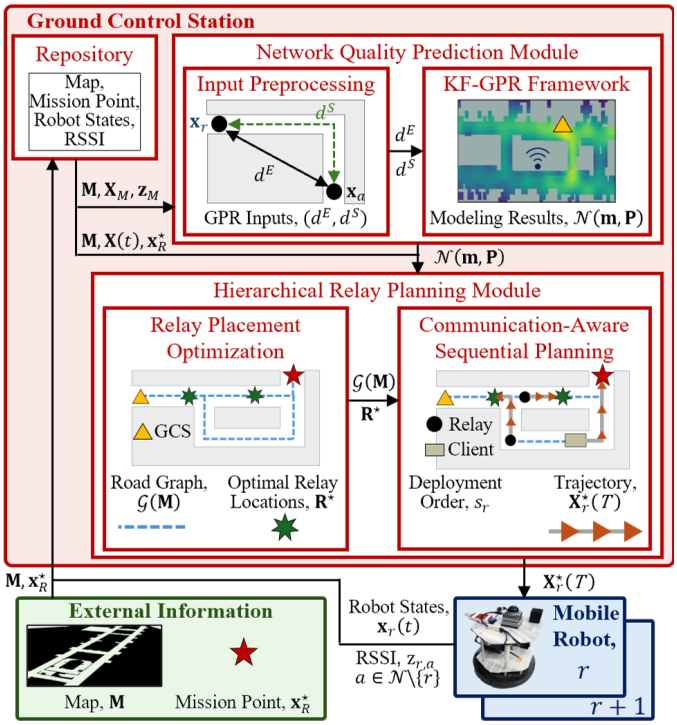

Fig. 2. The pipeline of the proposed system. The input map $(\mathbf{M})$ in the external information can be either a static prior map or one that is updated online. The system processes inputs such as the indoor map $(\mathbf{M})$, mission point $(\mathbf{x}^\star_R)$, each robot states $\mathbf{x}_r(t)$, and RSSI measurements $z_{r,a}$ through two core modules. The network quality prediction module generates a probabilistic network quality model $\mathcal{N}(\mathbf{m}, \mathbf{P})$. The hierarchical relay planning module then uses this model to compute optimal relay locations $(\mathbf{R}^\star)$ and communication-aware trajectories $(\mathbf{X}^\star_r(T))$ as the final output.

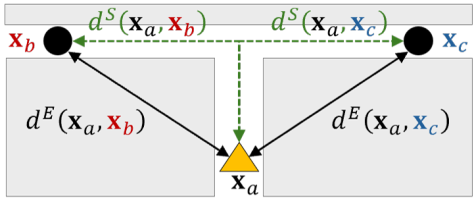

Fig. 3. A spatial correlation example of two different node pairs.

A. Real-Time Network Quality Prediction Model

1) Reduced Training Input Dimension: Conventional GPR for RSSI (3) uses absolute node coordinates $\mathbf{x}_{a,b} = [x_a, y_a, x_b, y_b]^\mathsf{T}$, which demands dense coverage and generalizes poorly indoors, where walls constrain propagation and relative geometry dominates. As illustrated in Fig. 3, pairs $(\mathbf{x}_a, \mathbf{x}_b)$ and $(\mathbf{x}_a, \mathbf{x}_c)$ can share the same d^E and d^S, yielding similar RSSI despite different absolute locations—yet a model trained only on $\mathbf{x}_{a,b}$ does not generalize to $\mathbf{x}_{a,c}$. We therefore replace absolute positions with the 2D feature $\mathbf{d}_{a,b} = [d^E_{a,b}, \bar{d}_{a,b}]^\mathsf{T}$ derived from the dominant path model (1). This compact input preserves propagation-relevant structure and improves GPR generalization, enabling accurate RSSI prediction even with less training data.

2) Concurrent GPR Training and RSSI Parameter Optimization: To train the GPR model in (3) and optimize the

IEEE Robotics and Automation Letters (RA-L) paper, presented at ICRA 2026, Vienna, Austria. Cite as RA-L paper.

RSSI parameters in (4), the conventional network quality prediction model suffers from a complexity of $\mathcal{O}(M^3)$ with respect to the training data size M. As the client continues its task and communicates through the relay robot, the RSSI measurements are gathered at diverse locations, causing the dataset to grow and making real-time prediction difficult. To mitigate this complexity issue, we adopt the KF-GPR framework proposed in [4]. The KF-GPR recasts kernel-based GPR (3) as a nonlinear regression using eigenfunctions $\boldsymbol{\phi}(\cdot)$ and the corresponding eigenvalues Λ of the kernel, allowing efficient recursive Bayesian inference. The derivation of eigenfunctions and eigenvalues can be found in [4].

In the KF-GPR framework, the latent function $f(\mathbf{x})$ in (2) is approximated by the finite-dimensional expansion $f(\mathbf{x}) = \boldsymbol{\phi}(\mathbf{x})^\mathsf{T}\mathbf{w}$, where $\mathbf{w} \in \mathbb{R}^E$ denotes the weight vector and $\boldsymbol{\phi}(\mathbf{x}) \in \mathbb{R}^E$ is the finite eigenfunction vector associated with the kernel in (3). This representation allows the model to be written in a state-space form and updated recursively with the Kalman filter. To jointly estimate the regression weights (GPR training) and the RSSI parameters, we define an augmented state vector $\bar{\mathbf{w}} = \left[\mathbf{w}^\mathsf{T}, n, \alpha\right]^\mathsf{T}$. For each new RSSI observation z_i at distance vector $\mathbf{d}_i$ between two nodes, the measurement model becomes linear in the form of:

$$z_i = \boldsymbol{\phi}(\mathbf{d}_i)^\mathsf{T}\mathbf{w} + P(\mathbf{d}_i; n, \alpha) + \epsilon = \mathbf{H}_i\bar{\mathbf{w}} + \epsilon, \tag{7}$$

where $\mathbf{H}_i = \left[\boldsymbol{\phi}(\mathbf{d}_i)^\mathsf{T}, -10\log_{10}(d_i^E), -\log_{10}(\bar{d}_i)\right]$. Starting from the prior $\bar{\mathbf{w}} \sim N(\mathbf{m}_0, \mathbf{P}_0)$, with $\mathbf{m}_0 = \mathbf{0}$ and $\mathbf{P}_0 = \Lambda = diag(\lambda_1, \ldots, \lambda_E)$, where $\lambda_1, \ldots, \lambda_E$ are the eigenvalues of the chosen kernel function, the posterior is updated through the Kalman filter recursions:

$$\mathbf{K}_i = \mathbf{P}_{i-1}\mathbf{H}_i^\mathsf{T}(\mathbf{H}_i\mathbf{P}_{i-1}\mathbf{H}_i^\mathsf{T} + \sigma_n^2)^{-1}, \tag{8}$$

$$\mathbf{m}_i = \mathbf{m}_{i-1} + \mathbf{K}_i(z_i - P_0 - \mathbf{H}_i\mathbf{m}_{i-1}), \tag{9}$$

$$\mathbf{P}_i = (\mathbf{I} - \mathbf{K}_i\mathbf{H}_i)\mathbf{P}_{i-1}. \tag{10}$$

where σ_n is the measurement noise in (2). For a query input $\mathbf{d}^* = [d^{E,*}, \bar{d}^*]^\mathsf{T}$, the predictive mean and variance are represented as:

$$\hat{\mu}(\mathbf{d}^*) = \boldsymbol{\phi}(\mathbf{d}^*)^\mathsf{T}\mathbf{m}_i, \quad \hat{\sigma}^2(\mathbf{d}^*) = \boldsymbol{\phi}(\mathbf{d}^*)^\mathsf{T}\mathbf{P}_i\boldsymbol{\phi}(\mathbf{d}^*). \tag{11}$$

With this proposed network quality prediction model, the computational complexity is significantly reduced in two aspects. First, the Kalman gain (8) requires only a scalar inversion of $(\mathbf{H}_i\mathbf{P}_{i-1}\mathbf{H}_i^\mathsf{T} + \sigma_n^2)$, eliminating expensive matrix inversions and making each update independent of M. Second, GPR training and RSSI parameters optimization are integrated into a single recursive operation, so no separate log-likelihood maximization is needed. These advantages enable constant-time updates and significantly enhance computational efficiency, supporting real-time network quality prediction over long mission execution.

The prediction results (11) are used to assess if the communication constraints in (6) are satisfied. Following previous studies [12], we use the cumulative distribution function (CDF) $F(\eta \mid \hat{\mu}(\mathbf{d}^*), \hat{\sigma}^2(\mathbf{d}^*))$ to estimate the probability of exceeding a predefined threshold η. Specifically, the predicted RSSI between nodes a and b, denoted $\hat{P}_{a,b}$, is modeled as a Gaussian random variable of the proposed network quality prediction model (11). Therefore, $Pr[\hat{P}_{a,b} \geq \eta] = 1 - F(\eta|\hat{\mu}(\mathbf{d}^*), \hat{\sigma}^2(\mathbf{d}^*))$ quantifies the probability that the predicted RSSI exceeds the threshold. To ensure reliable communication, this probability must exceed a minimum threshold θ to satisfy the constraints with high confidence.

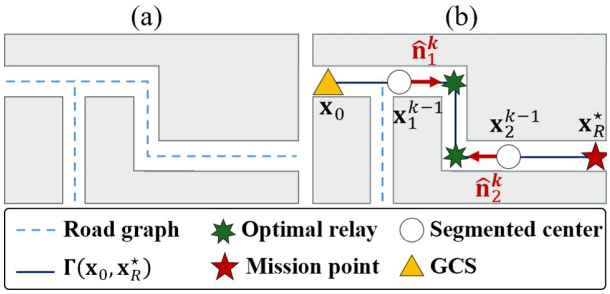

Fig. 4. (a) Extracted road graph. (b) Virtual force-based optimization for improving network quality.

B. Hierarchical Communication Relay Planning

As discussed in Section I, in environments where the client robot's mission point changes frequently, solving the optimization problem (6) requires identifying the shortest paths from the mission point to the GCS and subsequently determining appropriate relay locations. After that, mobile robots (client and relay robots) must be guided toward both the mission point and the selected relay locations, ensuring end-to-end connectivity [16], [17].

1) Relay Placement Optimization: While sampling-based methods are often used for shortest path computation, they tend to overlook corridor structures in indoor environments, resulting in inefficient planning. To address this limitation, we employ a road graph construction method $\mathcal{G}(\cdot)$ based on a skeleton extraction algorithm widely used in image processing [21], as in Fig. 4(a). By leveraging the structural characteristics of the indoor corridors, the road graph effectively compresses the feasible robot state space toward the central lines of the corridors. This enables more efficient relay location planning by substantially reducing the overall search complexity. Based on the road graph, we identify the shortest path $\Gamma^\star(\mathbf{x}_0, \mathbf{x}_R^\star)$ from a GCS to a mission point, and evenly segment it into intervals based on the number of relay robots. However, these may not provide optimal communication performance due to environmental complexities. To compensate for this, we apply a refinement process identifying optimal relay candidates via a virtual force derived from the RSSI differences between neighboring nodes, as in [14]. The optimal candidate update of the relay robot r at iteration k, denoted as $\mathbf{x}_r^k$, is guided by:

$$\mathbf{x}_r^k = \mathbf{x}_r^{k-1} + \beta \cdot P_{r,\text{diff}}\hat{\mathbf{n}}_r^k, \tag{12}$$

where, $P_{r,\text{diff}} = |\hat{P}_{r-1,r} - \hat{P}_{r,r+1}|$ represents the RSSI difference to neighbors, β is a step size, and $\hat{\mathbf{n}}_r^k$ indicates the RSSI gradient direction for robot r at iteration k, as in Fig. 4(b). The iterative update proceeds until a stopping condition is met—either a maximum iteration budget B_v is reached or the displacement between consecutive updates falls below a prescribed tolerance ν—thereby ensuring practical convergence. Then, we define the target locations of the client (mission point) and relay robots (relay locations), represented as $\mathbf{R}^\star = \{\mathbf{x}_r^\star | r \in \mathcal{N}\backslash\{0\}\}$.

IEEE Robotics and Automation Letters (RA-L) paper, presented at ICRA 2026, Vienna, Austria. Cite as RA-L paper.

2) Communication-Aware Sequential Planning: To minimize travel costs for deploying the relay robots to their relay locations, we formulate a standard task allocation problem using binary variables a_{rl}, where $a_{rl} = 1$ indicates that robot r is assigned to the relay location $\mathbf{x}_l^\star$, defined as:

$$\min \sum_{r=1}^{R-1} \sum_{l=1}^{R-1} d^S(\mathbf{x}_r, \mathbf{x}_l^\star) a_{rl}, \tag{13}$$

subject to the constraints that each relay robot is assigned to one unique relay location, and each relay location is assigned to one relay robot. This assignment problem is solved using the Hungarian algorithm [22], guaranteeing a unique assignment that minimizes the total travel distance. The resulting assignment yields a deployment sequence, which forms a permutation of relay robot indices, where s_r denotes the l-th relay location assigned to robot r:

$$s_r = \arg\max_l a_{rl}, \quad l \in \mathcal{N}_{\text{relay}}. \tag{14}$$

With the deployment sequence $\mathcal{S} = (s_0, s_1, \ldots, s_{R-1}, s_R)$ (including GCS $s_0 = 0$ and client $s_R = R$), we can plan a more cost-effective relay strategy.

After assigning each relay robot to a location $\mathbf{x}_r^\star$, we must guide it to the target while ensuring the end-to-end network quality $\hat{P}_c$ remains above a threshold η. Thus, the optimization problem (6) is reformulated as follows:

$$\begin{aligned} \mathbf{X}^\star(\mathcal{T}) = \arg\min_{\mathbf{X}(\mathcal{T})} & \textstyle\sum_{r=1}^{R} \int_{\mathcal{T}} ||\dot{\mathbf{x}}_r(t)|| dt + \gamma \Psi(\mathbf{x}_r), \\ s.t. \;\; & Pr[\hat{P}_c(\mathbf{X}(t)) \geq \eta] \geq \theta, \;\; \forall t \in \mathcal{T}. \end{aligned} \tag{15}$$

where $\Psi(\mathbf{x}_r) = d^S(\mathbf{x}_r(t_f), \mathbf{x}_r^\star)$. Since $\hat{P}_c(\mathbf{X}(t))$ is determined by the minimum RSSI along the chain, we simplify the joint optimization problem in (15) by adopting a sequential planning approach, where robots move one by one starting from the one nearest the GCS. This decomposition reduces planning complexity while maintaining the connectivity guarantee. Obtaining real-time solutions of multi-robot trajectory finding in continuous time is known as NP-hard [23]. We thus discretize the time domain $T = \{0, \ldots, t_f\}$, formulating each robot's optimization problem:

$$\begin{aligned} \mathbf{X}_r^\star(\mathcal{T}) = \arg\min_{\mathbf{X}_r(T)} & \textstyle\sum_{t=0}^{t_f-1} d^S(\mathbf{x}_r(t), \mathbf{x}_r(t+1)) + \gamma \Psi(\mathbf{x}_r), \\ s.t. \;\; & Pr[\hat{P}_{r-1,r} \geq \eta] \geq \theta, \;\; \forall t \in T. \end{aligned} \tag{16}$$

To solve the optimization problem in (16), we adopt the MCTS algorithm, which is effective for real-time planning in discrete action spaces by balancing exploration and exploitation through a tree-based simulation [5]. Since we guide each robot to operate on the road graph, the action space is determined within the road graph. For each robot r, we first extract traversable trajectories $\{\mathbf{X}_r^j(T)\}_{j \in J}$, where each trajectory $\mathbf{X}_r^j(T) = \{\mathbf{x}_r^j(t)\}_{t=0}^{t_f}$ consists of uniformly discretized waypoints connecting the robot's current location $\mathbf{x}_r(0)$ to its assigned target $\mathbf{x}_r^\star$ on the road graph. Here, J denotes the set of all possible routes. The MCTS algorithm explores discretized action spaces up to B_{mcts} iterations via selection, simulation, and back-propagation. Each node in the MCTS tree corresponds to a specific robot state $\mathbf{x}_r^j(t)$ at time t along a candidate trajectory $\mathbf{X}_r^j(T)$. That is, a node represents a discretized state in space and time from which subsequent actions can be simulated. In the selection step, the algorithm balances exploration and exploitation to choose an action from the currently expanded tree. This is achieved using the upper confidence bound (UCT) rule:

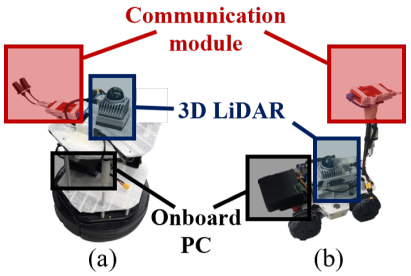

Fig. 5. Physical platforms for the experiments. (a) Turtlebot 2. (b) LiMO.

$$\mathbf{UCT}(\mathbf{x}_r^j(t)) = \bar{Q}(\mathbf{x}_r^j(t)) + C_p \sqrt{\frac{2 \log V(\mathbf{x}_r^j(t-1))}{V(\mathbf{x}_r^j(t))}}, \tag{17}$$

where $V(\cdot)$ denotes the visit count of a node, and C_p is a balancing parameter. To compute the average reward $\bar{Q}(\mathbf{x}_r^j(t))$, the instance reward $Q(\mathbf{x}_r^j(t))$ is designed as:

$$Q(\mathbf{x}_r^j(t)) = \begin{cases} 1 - \frac{d^S(\mathbf{x}_r^j(t), \mathbf{x}_r^\star)}{\hat{d}_r^S}, & \text{if } Pr\left[\hat{P}_{r-1,r} \geq \eta\right] \geq \theta, \\ -1, & \text{otherwise}, \end{cases}$$

where $d^S_{\mathbf{X}_r^j(T)} = \sum_{t=0}^{t_f-1} d^S\left(\mathbf{x}_r^j(t), \mathbf{x}_r^j(t+1)\right)$ is the length of the selected trajectory $\mathbf{X}_r^j(T)$, and $\hat{d}_r^S = \max_{j \in J} \{d^S_{\mathbf{X}_r^j(T)}\}$. This reward encourages progress toward $\mathbf{x}_r^\star$ while penalizing any step that violates the network quality constraint with the preceding robot $r-1$. If the selected node has no children, a random node is simulated up to a rollout length equal to the discretized final time t_f. Finally, the reward and visit count of each node are updated according to the explored action sequences. Through these cyclic processes, each robot sequentially identifies the best trajectory according to (16).

V. Results

This section evaluates the proposed system through simulations and experiments, focusing on the accuracy of the network quality prediction and the effectiveness of the hierarchical relay planning.

For the experiments, we used the physical platforms shown in Fig. 5. While the proposed system is platform-agnostic, our heterogeneous setup consisted of a LiMO as the client and Turtlebot 2 as relays, each equipped with an Intel NUC13ANKi5. To ensure network consistency, identical Rajant Cardinal modules were mounted on all robots and the GCS, supporting dynamic mesh networking capabilities. FAST-LIO [24] handles localization with a Livox MID-360 LiDAR. The key parameters, presented in Table I, were heuristically chosen to ensure both high performance and real-time feasibility.

A. Network Prediction Models Performance

1) Computation complexity analysis: We evaluated the proposed network quality prediction model through signal estimation simulations using RSSI measurements. A representative environment along with randomly sampled data utilized for training GPR models is illustrated in Fig. 6(a). In this scenario,

IEEE Robotics and Automation Letters (RA-L) paper, presented at ICRA 2026, Vienna, Austria. Cite as RA-L paper.

TABLE I
PARAMETERS OF COMMUNICATION RELAY SYSTEMS

Parameter	Value
Network Quality Prediction Model	
The number of eigenfunctions, E	800
Measurement noise, σ_n	3(dBm)
Reference signal strength, P_0	-30(dBm)
Hierarchical Planning	
(Virtual force) Step-size, β	2.0
(Virtual force) Tolerance, ν	1.5(dBm)
(Virtual force) Maximum iterations, B_v	1000
(MCTS) Maximum iterations, B_{mcts}	300
(MCTS) Rollout length, t_f	5
(MCTS) Balancing coefficient, C_p	1.0
(MCTS) RSSI threshold, η	-85(dBm)
(MCTS) Empirical probability threshold, θ	0.75

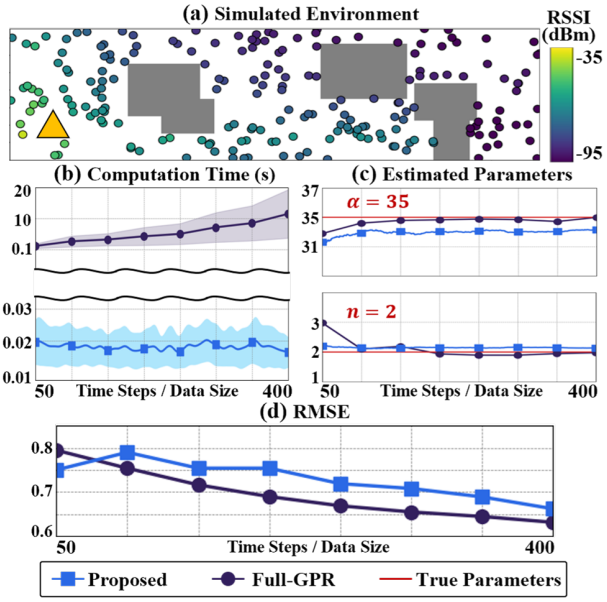

Fig. 6. Performance comparison of the proposed model with the conventional Full-GPR. (a) Indoor simulation environment with a GCS (yellow triangle). (b) Average model-update computation time. (c) Convergence of the estimated RSSI parameters n and α. (d) RMSE of each model.

20 independent trials were conducted to assess and compare the performance of both the conventional Full-GPR and the proposed model. The Full-GPR retrains the entire dataset whenever new data is obtained; however, due to its high computational load, retraining (including both RSSI parameter optimization and model update) is restricted to intervals of every 50 newly acquired measurements. In contrast, the proposed model immediately incorporates each new measurement into the model by simultaneously updating the proposed model and optimizing the RSSI parameters (n, α) in a single step. Both prediction models optimize the RSSI parameters starting from the initial values $(4, 30)$.

A comparison of the computation time and the parameter estimation accuracy is presented in Fig. 6(b) and Fig. 6(c). Full-GPR exhibits slightly lower estimation errors; however, its computational load grows significantly with dataset size, quickly exceeding practical real-time constraints. On the other hand, the proposed model demonstrates stable computational efficiency, consistently maintaining an average processing time of approximately $0.02s$ per update, regardless of the expansion of the data set. The root mean squared error (RMSE) of each

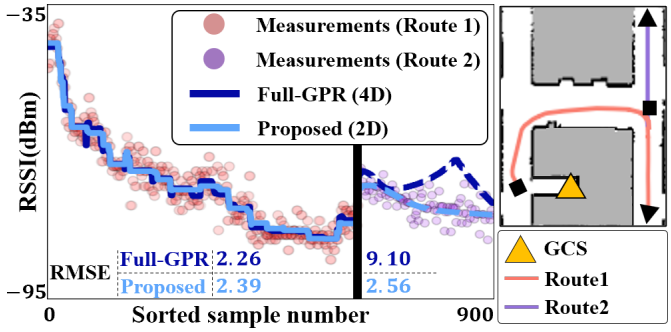

Fig. 7. Comparison of RSSI prediction results using experiment data. The right panel illustrates the actual robot routes, where black rectangles denote the starting points and black triangles indicate the endpoints for each route. In the left panel, solid lines indicate predictions within regions covered by training data (Route 1), while dashed lines represent predictions in regions where no measurements were used for model training (Route 2).

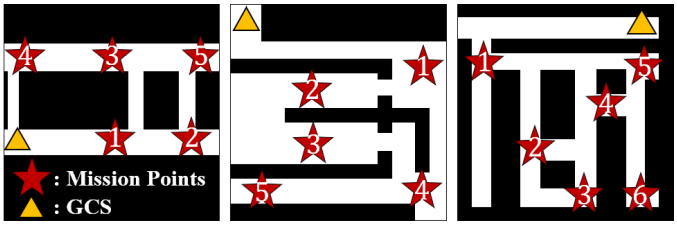

Fig. 8. Synthesized indoor environments used for simulations (Env 1 to 3, from left to right).

model relative to the ground truth was also evaluated on 400 randomly generated test points, as shown in Fig. 6(d). While the Full-GPR achieves a lower RMSE by estimating model parameters more precisely, our model delivers sufficiently optimized results with real-time capability, making it more practical for online applications.

2) Predictive accuracy with empirical data: To compare the prediction performance of the proposed network quality model with that of Full-GPR, the client robot collected RSSI data along predefined paths, as illustrated in Fig. 7. In the left panel, the red-colored measurements correspond to the data collected along Route 1, while the purple-colored measurements were obtained along Route 2. These measurements provide spatial context for the sorted data, illustrating how the signal strength changes as the robot traverses each route.

Both models performed similarly within the training region (Route 1), accurately tracking the measured RSSI. However, in the test region (Route 2), the proposed model outperformed Full-GPR. By using reduced 2D input features that capture spatial similarity, the proposed model generalized better to unseen data with an RMSE of 2.56. In contrast, Full-GPR exhibited degraded performance with an RMSE of 9.10, likely due to overfitting on less informative features. This highlights the potential of the proposed model for accurate RSSI prediction in complex indoor environments, enabling reliable signal-based navigation through robust network quality prediction.

B. Communication Relay System Validation

1) Simulations with synthesized indoor environments: To assess how the network prediction accuracy influences the proposed communication-aware planner, we simulated three $55(m) \times 55(m)$ synthesized indoor environments (Fig. 8). In

IEEE Robotics and Automation Letters (RA-L) paper, presented at ICRA 2026, Vienna, Austria. Cite as RA-L paper.

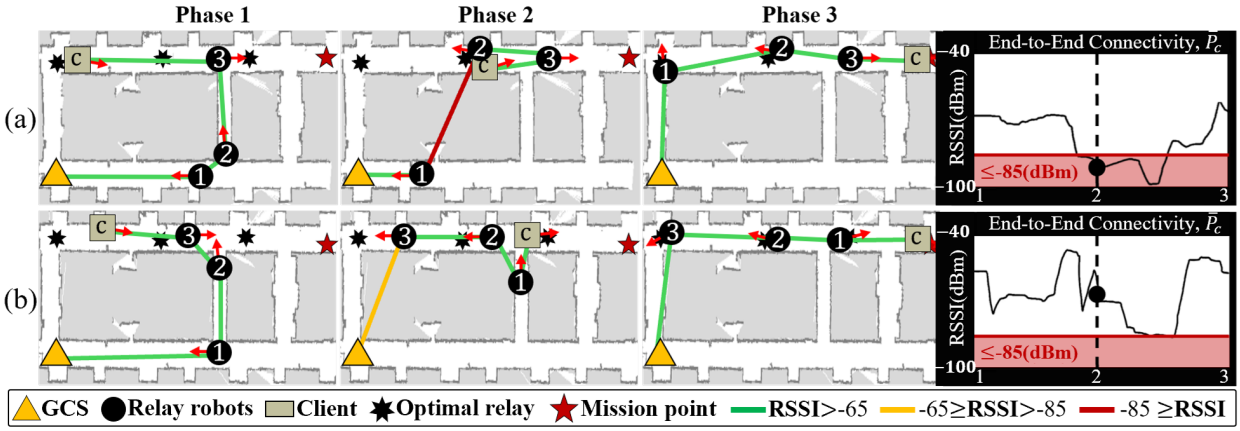

Fig. 9. Illustrative example of two algorithms during exploration tasks. Each relay robot is labeled with a number, and the client is labeled c. (a) Baseline. (b) The proposed hierarchical planning strategy.

TABLE II
CHANNEL RELIABILITY (CR) RESULTS IN SIMULATIONS

	Env 1	Env 2	Env 3
Full-GPR ($\sigma_n = 10$)	93.1(%)	85.6(%)	85.8(%)
Full-GPR ($\sigma_n = 3$)	97.1(%)	92.8(%)	91.4(%)
Proposed ($\sigma_n = 10$)	94.9(%)	92.2(%)	92.6(%)
Proposed ($\sigma_\mathbf{n} = 3$)	**99.0(%)**	**98.7(%)**	**99.1(%)**

each run, a client and three relay robots were initially deployed near the GCS, and the client sequentially visited the mission points. Channel reliability (CR) quantifies the temporal availability of the network, representing the percentage of total time that the $\bar{P}_c(\mathbf{X}(t)) \geq \eta$. Each model was trained on RSSI measurements corrupted with $\sigma_n \in \{3, 10\}$.

Results in Table II show that lower prediction accuracy (larger σ_n) increases discrepancy between predicted and measured network quality, leading to constraint violations at execution time and thus reduced CR. This degradation is exacerbated in more complex environments where network quality varies unpredictably with position, so constraints satisfied during the planning phase are more often violated in deployment. Across all environments and noise levels, the proposed network prediction model generalizes better than Full-GPR, yielding consistently higher CR; notably, Full-GPR degrades from Env 1 to Env 2–3, whereas the proposed model—especially when trained with low-noise measurements—maintains higher reliability and exhibits stronger robustness to environmental variation.

2) Real-world validation with an indoor exploration task: We validated the proposed relay system's performance in a real-world scenario that exemplifies a dynamic mission. The experiment was conducted in a $55(m) \times 15(m)$ indoor environment, which is particularly challenging for radio propagation due to its windowless corridors and non-traversable concrete structures. For this validation, the client robot performed a frontier-based exploration task [25], a dynamic mission where the robot's goal is constantly updated as it maps an unknown area. A client robot built an occupancy map and transmitted it to a GCS via a chain of three relay robots. Based on this scenario, we conducted a comparative study against a baseline algorithm. A survey noted that for exploration tasks involving a single client robot, an advantageous strategy is to establish a multi-hop chain between the GCS and the frontier,

TABLE III
COMMUNICATION PERFORMANCE ANALYSIS

	Baseline		Proposed	
	CR(%)	PDR(%)	CR(%)	PDR(%)
Trial 1	86.3	31.2	99.3	73.8
Trial 2	90.9	51.1	99.1	72.1
Trial 3	92.4	54.6	99.3	80.3
Trial 4	88.7	51.4	98.8	67.1
Trial 5	86.6	35.6	99.0	75.4
Avg.	88.9	44.7	99.1	73.7

deploying relay robots based on the signal quality between adjacent nodes [23]. Therefore, we selected a similar method in [14] as our baseline. To adapt [14] to dynamically changing missions, its optimal relay locations were computed between the GCS and the mission point. Each algorithm was executed in five independent tests with different initial placements of the relay robots. CR and packet delivery ratio (PDR) are used to capture two complementary aspects of communication performance. PDR represents the proportion of successfully delivered occupancy grid map packets:

$$\text{PDR} = (N_{\text{received}}/N_{\text{sent}}) \times 100\ (\%), \tag{18}$$

where N_{received} and N_{sent} denote the numbers of received and sent packets, respectively.

With the proposed sequential planning strategy, each robot's trajectory is generated using MCTS under an explicit network quality constraint. This allows the robots to actively avoid network outages that the baseline method ignores. As shown in Table III, the proposed hierarchical planning consistently maintained CR above $98.8(\%)$ across all trials, while the baseline method achieved only up to $92.4(\%)$, with the lowest performance at $86.3(\%)$. A similar trend is observed for PDR, which increased from 31-55$(\%)$ in the baseline to 67-80$(\%)$ under the proposed strategy. The observed positive correlation between CR and PDR implies that sustained network availability enables more opportunities for successful packet forwarding. Moreover, the relatively larger improvement in PDR suggests that the proposed method not only avoids disconnection but also mitigates packet loss, thereby enhancing the continuity of data exchange.

The snapshots and RSSI traces in Fig. 9 show representative moments from the fifth trial of each method, selected to highlight key differences between the baseline and the pro-

IEEE Robotics and Automation Letters (RA-L) paper, presented at ICRA 2026, Vienna, Austria. Cite as RA-L paper.

posed strategy. In the baseline, relay robot 1 initially detours and drifts away from the rest of the robots, causing a steep RSSI drop, as indicated by the corresponding RSSI trace on the right panel of Fig. 9(a). In contrast, as shown in Fig. 9(b), although robot 1 initially moves away from the GCS, robot 3 compensates by positioning itself closer to the GCS, thereby preserving the end-to-end connectivity. This adaptive deployment behavior results from combining a deployment ordering with an MCTS-based sequential planner, which together guide each relay robot to its optimal location while preserving continuous connectivity. By minimizing travel cost and enforcing connectivity constraints during planning, the proposed method enables robust coordination among relay robots, significantly reducing the frequency and duration of RSSI drops below the critical threshold.

VI. Conclusions and Future Work

This letter presents a real-time communication-relay system that couples a low-complexity network quality prediction model with a hierarchical relay planner tailored to dynamic indoor missions. The proposed prediction model achieves constant-time updates ($\sim 0.02s$) regardless of dataset growth, enabling online operation, while maintaining competitive model accuracy. In generalization tests with empirical data, the proposed model achieved RMSE of 2.56 on an unseen route, compared with 9.10 for Full-GPR, indicating stronger robustness to spatial variability. In simulation across three indoor layouts, the proposed model sustained higher CR than Full-GPR under both low and high noise training conditions, highlighting robustness to environmental complexity. Finally, in real-world exploration with a chain of three relays, our sequential MCTS-based planner consistently maintained CR$\geq$ 98.8% and improved the PDR from 44.7% to 73.7% on average, demonstrating a practical advantage over a virtual-force chain baseline.

While the proposed sequential planner ensures connectivity at discrete time steps, it does not explicitly guarantee connectivity between these steps. This limitation is evidenced by the channel reliability results in Table II and Table III, where values occasionally fall below 100%, indicating intermittent disconnections can still occur. Future work could incorporate local planning to bridge these gaps and generate continuous, communication-preserving trajectories. Furthermore, the current system is limited to environments with static obstacles, presenting an opportunity to extend the methodology to time-varying settings. Such an extension could involve integrating an augmented network quality prediction model with time-dependent features and a more reactive planner capable of anticipating potential communication blockages.

References

[1] M. Tranzatto, T. Miki, M. Dharmadhikari, L. Bernreiter, M. Kulkarni, F. Mascarich, O. Andersson, S. Khattak, M. Hutter, R. Siegwart, *et al.*, "Cerberus in the DARPA subterranean challenge," *Sci. Robot.*, vol. 7, no. 66, pp. 1–6, 2022.

[2] F. Amigoni, J. Banfi, and N. Basilico, "Multirobot exploration of communication-restricted environments: A survey," *IEEE Intell. Syst.*, vol. 32, no. 6, pp. 48–57, 2018.

[3] A. Cid, A. Vangasse, S. Campos, M. Delunardo, G. Cruz Junior, N. Neto, L. Pimenta, J. Domingues, L. Barros, H. Azpúrua, *et al.*, "Wireless communication-aware path planning and multiple robot navigation strategies for assisted inspections," *J. Intell. Robot. Syst*, vol. 110, no. 2, pp. 88–107, 2024.

[4] A. Solin, M. Kok, N. Wahlström, T. B. Schön, and S. Särkkä, "Modeling and interpolation of the ambient magnetic field by Gaussian processes," *IEEE Trans. Robot.*, vol. 34, no. 4, pp. 1112–1127, 2018.

[5] L. Kocsis and C. Szepesvári, "Bandit based Monte-Carlo planning," in *Eur. Conf. Mach, Learn.*, 2006, pp. 282–293.

[6] J. Kim, P. Ladosz, and H. Oh, "Optimal communication relay positioning in mobile multi-node networks," *Robot. Auton. Syst.*, vol. 129, p. 103517, 2020.

[7] ITU-R, "Propagation data and prediction methods for the planning of indoor radiocommunication systems and radio local area networks in the frequency range 900 MHz to 100 GHz, Tech. Rep. Recommendation ITU-R P.1238-7, 2012.

[8] H. Obeidat, A. Alabdullah, E. Elkhazmi, W. Suhaib, O. Obeidat, M. Alkhambashi, M. Mosleh, N. Ali, Y. Dama, Z. Abidin, *et al.*, "Indoor environment propagation review," *Comput. Sci. Rev.*, vol. 37, pp. 1–22, 2020.

[9] J. Hoydis, F. Aït Aoudia, S. Cammerer, M. Nimier-David, N. Binder, G. Marcus, and A. Keller, "Sionna RT: Differentiable ray tracing for radio propagation modeling," in *IEEE Globecom Workshops*, 2023, pp. 317–321.

[10] H. A. Obeidat, R. Asif, N. T. Ali, Y. A. Dama, O. A. Obeidat, S. M. R. Jones, W. S. Shuaieb, M. A. Al-Sadoon, K. W. Hameed, A. A. Alabdullah, *et al.*, "An indoor path loss prediction model using wall correction factors for wireless local area network and 5g indoor networks," *Radio Sci.*, vol. 53, no. 4, pp. 544–564, 2018.

[11] L. Clark, J. A. Edlund, M. S. Net, T. S. Vaquero, and A. A. Agha-Mohammadi, "Propem-l: Radio propagation environment modeling and learning for communication-aware multi-robot exploration," in *Robot.: Sci. Syst.*, 2022.

[12] P. Ladosz, H. Oh, G. Zheng, and W. H. Chen, "Gaussian process based channel prediction for communication-relay UAV in urban environments," *IEEE Trans. Aerosp. Electron. Syst.*, vol. 56, no. 1, pp. 313–325, 2019.

[13] A. Quattrini Li, P. K. Penumarthi, J. Banfi, N. Basilico, J. M. O'Kane, I. Rekleitis, S. Nelakuditi, and F. Amigoni, "Multi-robot online sensing strategies for the construction of communication maps," *Auton. Robots*, vol. 44, pp. 299–319, 2020.

[14] Y. Gao, H. Chen, Y. Li, C. Lyu, and Y. Liu, "Autonomous Wi-Fi relay placement with mobile robots," *IEEE/ASME Trans. Mechatron.*, vol. 22, no. 6, pp. 2532–2542, 2017.

[15] P. Laclau, V. Tempez, F. Ruffier, E. Natalizio, and J. B. Mouret, "Signal-based self-organization of a chain of UAVs for subterranean exploration," *Front. Robot. AI*, vol. 8, p. 614206, 2021.

[16] V. S. Varadharajan, D. St-Onge, B. Adams, and G. Beltrame, "Swarm relays: Distributed self-healing ground-and-air connectivity chains," *IEEE Robot. Autom. Lett.*, vol. 5, no. 4, pp. 5347–5354, 2020.

[17] J. Stephan, J. Fink, V. Kumar, and A. Ribeiro, "Concurrent control of mobility and communication in multi-robot systems," *IEEE Trans. Robot.*, vol. 33, no. 5, pp. 1248–1254, 2017.

[18] G. Wölfle, R. Wahl, P. Wertz, P. Wildbolz, and F. Landstorfer, "Dominant path prediction model for indoor scenarios," in *Proc. German Microw. Conf.*, vol. 27, 2005, pp. 176–179.

[19] C. K. Williams and C. E. Rasmussen, *Gaussian processes for machine learning*. MIT press Cambridge, MA, 2006, vol. 2, no. 3.

[20] J. Fink and V. Kumar, "Online methods for radio signal mapping with mobile robots," in *IEEE Int. Conf. Robot. Autom.*, 2010, pp. 1–6.

[21] Z. Guo and R. W. Hall, "Parallel thinning with two-subiteration algorithms," *Commun. ACM*, vol. 32, no. 3, pp. 359–373, 1989.

[22] H. W. Kuhn, "The Hungarian method for the assignment problem," *Naval Res. Logist.*, vol. 2, no. 1-2, pp. 83–97, 1955.

[23] A. Muralidharan and Y. Mostofi, "Communication-aware robotics: Exploiting motion for communication," *Annu. Rev. Control Robot. Auton. Syst.*, vol. 4, no. 1, pp. 115–139, 2021.

[24] W. Xu and F. Zhang, "Fast-lio: A fast, robust LiDAR-inertial odometry package by tightly-coupled iterated Kalman filter," *IEEE Robot. Autom. Lett.*, vol. 6, no. 2, pp. 3317–3324, 2021.

[25] L. Freda and G. Oriolo, "Frontier-based probabilistic strategies for sensor-based exploration," in *IEEE Int. Conf. Robot. Autom.*, 2005, pp. 3881–3887.